Xiaofei Hu, Dianbao Chen, Baotian Pan, Jinjun Chen, Jian Zhang, Jing Chang, Changsheng Gong, and Qiming Zhao, 2019, Sedimentary evolution of the foreland basin in the NE Tibetan Plateau and the growth of the Qilian Shan since 7 Ma: GSA Bulletin, https://doi.org/10.1130/B35106.1.

Data Repository

1. MAGNETIC PARAMETERS

Analysis of magnetic parameters [Median destructive field (MDF), ΔGRM/ΔNRM, hysteresis parameters (Bc, Mrs/Ms) and NRM values] (Fig. DR1) indicates that there are no significant differences between normal and reverse polarity samples; in addition, there is no evidence of remagnetization. Additional details are given below.

i) Significant diagenetic greigite is indicated by high coercivity (Bc) values (often >35 mT), and a high ratio of saturation remanent magnetization to saturation magnetization (Mrs/Ms) (often >0.4) (Roberts et al., 1995; Roberts et al., 2011; Chang et al., 2008; Qiang et al., 2018). Greigite diagnostics are based on a Gyroremanent Magnetization (GRM) acquired perpendicular to the AF field direction during NRM demagnetization (Stephenson, 1980). The high GRM of greigite is unique among all known natural magnetic minerals and can be used to detect it (Fu et al., 2008; Roberts et al., 2011; Liu et al., 2014). The parameter ΔGRM/ΔNRM (Fu et al., 2008) is used to quantify the relative contribution of gyroremanence. ΔGRM is expressed as the difference between the final and minimum values of remanence intensity during AfD, while ΔNRM is the difference between the initial and minimum values of the remanence intensity during AfD.

Low Bc values (often <30 mT) and low Mrs/Ms ratios (<0.3) indicate the absence of significant diagenetic greigite in the MH core. Also, the hysteresis parameters (Bc, Mrs/Ms) reveal no conspicuous differences between neighboring samples with an opposite polarity and from the same lithology (Fig. DR1).

The ratios of ΔGRM/ΔNRM in the MH core also provide no indication of the significant occurrence of greigite, since no measurable GRM was apparent during AF demagnetization. Therefore, magnetite and/or hematite carry the primary depositional remanent magnetization.

ii) In general, there is no correlation between the polarity column and NRM variability (typically 10^{-4}–10^{-2} A/m) (Fig. DR1); in addition, the normal magnetozones are not characterized by unusual NRM values. This implies the absence of remagnetization effects. In addition, the median destructive field (MDF) of the AF-demagnetized samples is typically ≤25 mT (Fig. DR1), except for some samples with MDF >30 mT. There are no large differences between normal and reverse polarity samples in terms of MDF (Fig. DR1).

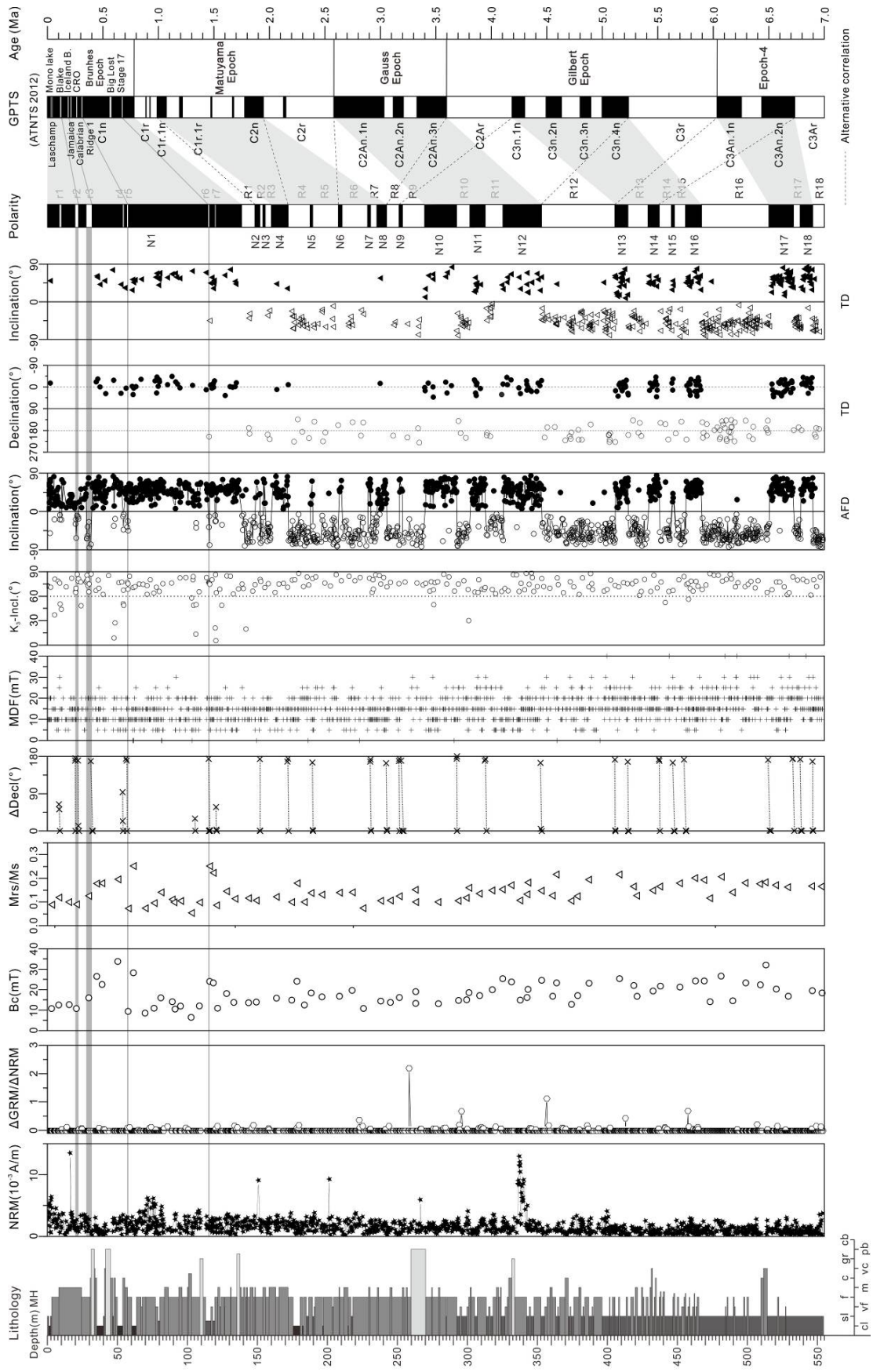
Age (Ma)
GPTS (ATNTS 2012)
Mono lake
Blake
Iceland B.
CRO
Brunhes Epoch
Big Lost
Stage 17
Matuyama Epoch
Gauss Epoch
Gilbert Epoch
Epoch-4
Lascamp
Jamaica
Calabrian Ridge 1
C1n
C1r
C1r.1n
C1r.1r
C2n
C2r
C2An.1n
C2An.2n
C2An.3n
C2Ar
C3n.1n
C3n.2n
C3n.3n
C3n.4n
C3r
C3An.1n
C3An.2n
C3Ar
Polarity
Inclination(°)
Declination(°)
TD
AFD
K$_2$-Incl.(°)
MDF(mT)
ΔDecl(°)
Mrs/Ms
Bc(mT)
ΔGRM/ΔNRM
NRM(10^{-3}A/m)
Lithology
Depth(m) MH
Alternative correlation

Figure DR1. Magnetostratigraphic results for the MH core and its correlation with the geomagnetic polarity timescale (GPTS) (Gradstein et al., 2012). Short excursions are from Laj and Channell, 2007; Roberts, 2008; Singer, 2014. NRM–intensity of the natural remanent magnetization; ΔGRM–gyromagnetic remanence intensity acquired between the final and minimum values of the remanence intensity during AfD, ΔNRM–the difference between the initial and minimum values of the remanence intensity during AfD; Bc–coercivity, Mrs/Ms–ratio of saturation remanent magnetization to saturation magnetization; 'ΔDecl'–the angle of declination change in samples from the same core segment; we only used data from those segments in which polarity reversals were interpreted from inclination changes (the lowermost sample in the segment is set to 0° and the two subsequent samples upwards are expressed relative to the lowermost sample); MDF–median destructive field; K_3-incl.–inclination of the minimum susceptibility axis; AFD–alternating demagnetization; TD–thermal demagnetization.

2. χ–T CURVES

It is commonly observed that the oxidation of pyrite or the thermal decomposition of greigite during heating is accompanied by a sharp χ increase between 400 and 500 °C (Passier et al., 2001; Minyuk et al., 2013; Su et al., 2013; Fu et al., 2015). The shape of the χ–T heating curves (Fig. DR2; Figure 5 in the Manuscript) demonstrates that there is no significant occurrence of paramagnetic Fe sulfides.

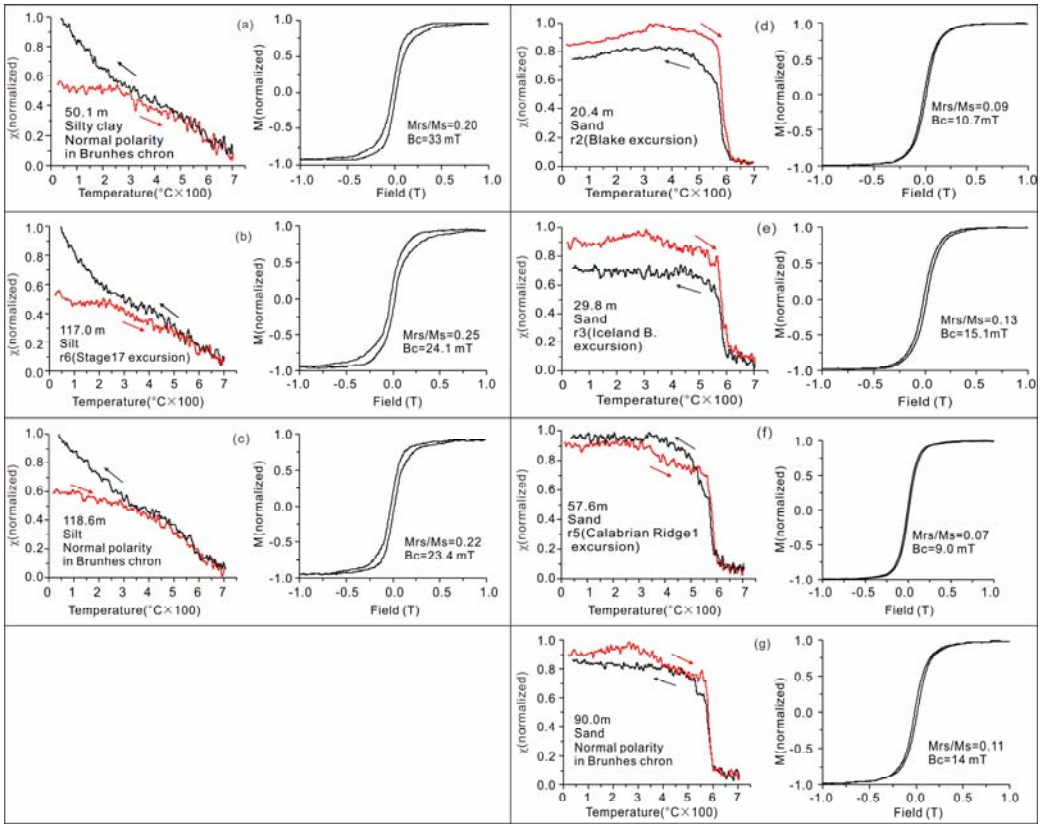

Figure DR2. Thermomagnetic curves (left in a, b, c, d, e, f and g) and magnetic hysteresis loops (right in a, b, c, d, e, f and g) for representative samples of different lithologies from Chron C1n (a, b and c–silty clay, silt; d, e, f and g–sand) from the MH core. The red line represents the heating curve and the black line represents the cooling curve.

3. REORIENTATION OF THE CORE

Reorientation of the MH core was carried out using the direction of the low temperature viscous components from 233 sedimentary samples with unambiguous orthogonal demagnetization characteristics (Fuller, 1969; Thibal et al., 1999; Ezquerro et al., 2016) (Fig. DR1; Fig. DR4). Samples with viscous components with ambiguous or noisy orthogonal demagnetization diagrams and negative inclination were rejected. The values of Fisher mean declination (D), inclination (I), precision parameter (k) and 95% confidence limits (α_{95}) of the corrected ChRM of positive (negative) polarity are 0.2°, 53.2°, 23.4 and 2.5° (184.6°, –56.1°, 17.3 and 4.2°), respectively (Fig. DR4). The corrected ChRM directions pass the reversal test despite deviation during coring, sampling errors and viscous remanence modification (McFadden and McElhinny, 1990; Tauxe, 1998) (Fig. DR4D). Moreover, the changes in the declination of the corrected ChRM are consistent with the inclination (Fig. DR1). This suggests that reorienting the MH core reinforces our magnetostratigraphic interpretations.

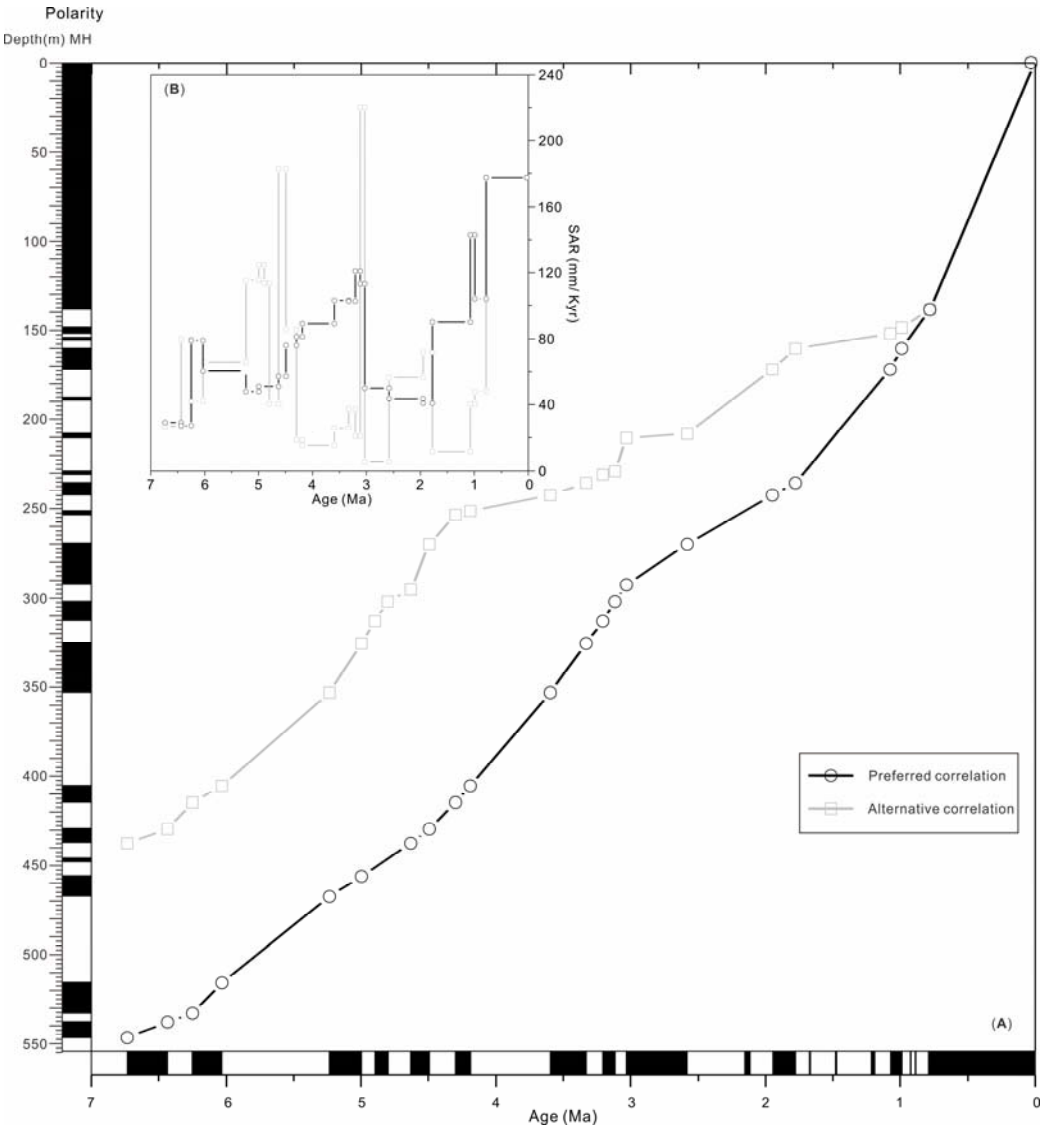

Figure DR3. Age versus depth plots (A) and sediment accumulation rates (SAR) (B) based on preferred and alternative correlations. The alternative correlation is shown in Figure DR1.

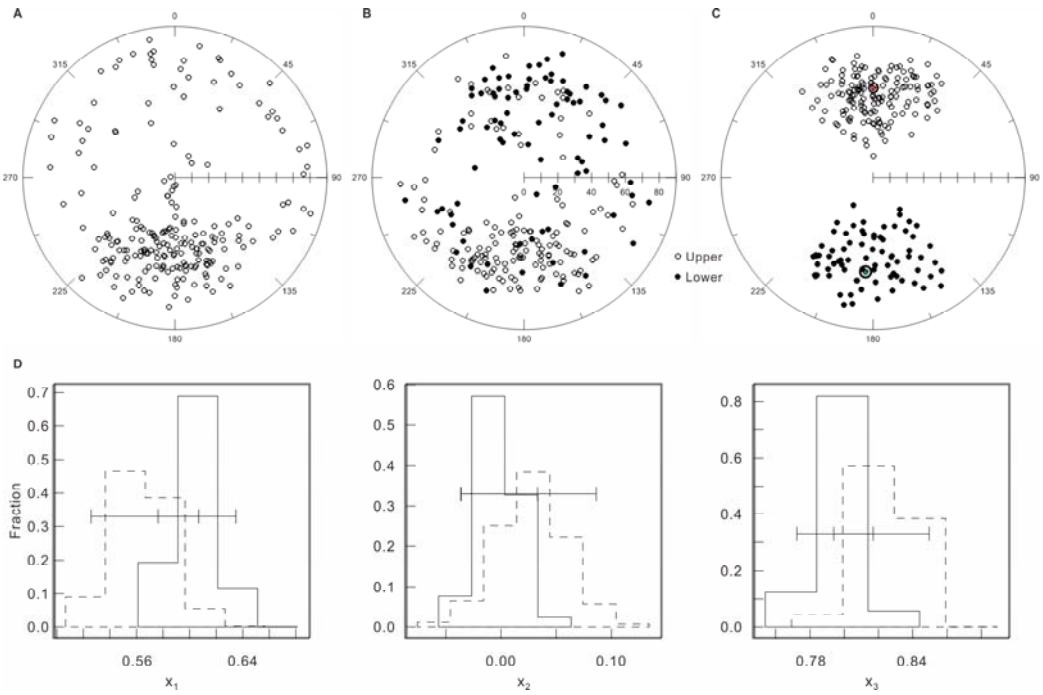

Figure DR4. Equal area projections of the uncorrected directions of the low-temperature remanent magnetization component (VRM) (A), pre-adjusted directions of the ChRM component (B) and ChRM after adjustment (C) of sedimentary samples from the MH core. (D) Reversal test diagram (Tauxe, 1998) of the ChRM. The black open circles (C) represent the mean directions of both polarities.

REFERENCES CITED

Chang, L., Roberts, A.P., Tang, Y., Rainford, B.D., Muxworthy, A.R., and Chen, Q., 2008, Fundamental magnetic parameters from pure synthetic greigite (Fe_3S_4): Journal of Geophysical Research, v. 113, p. B06104, doi:, https://doi.org/10.1029/2007JB005502.

Ezquerro, L., Moretti, M., Liesa, C.L., Luzón, A., et al., 2016, Controls on space-time distribution of soft-sediment deformation structures: applying palaeomagnetic dating to approach the apparent recurrence period of paleoseisms at the Concud Fault (eastern Spain): Sedimentary Geology, v. 344, p. 91–111, https://doi.org/10.1016/j.sedgeo.2016.06.007.

Fu, C.F., Bloemendal, J., Qiang, X.K., Hill, M.J., and An, Z.S., 2015, Occurrence of greigite in the Pliocene sediments of Lake Qinghai, China, and its paleoenvironmental and paleomagnetic implications: Geochemistry Geophysics Geosystems, v. 16, p. 1293–1306, doi:, https://doi.org/10.1002/2014GC005677.

Fu, Y.Z., Dobeneck, T.V., Franke, C., Heslop, D., and Kasten, S., 2008, Rock magnetic identification and geochemical process models of greigite formation in Quaternary marine sediments from the Gulf of Mexico (IODP Hole U1319A): Earth and Planetary Science Letters, v. 275, p. 233–245, https://doi.org/10.1016/j.epsl.2008.07.034.

Fuller, M., 1969, Magnetic orientation of borehole cores: Geophysics, v. 34, p. 772–774, https://doi.org/10.1190/1.1440047.

Gradstein, F.M., Ogg, J.G., Schmitz, M.D., and Ogg, G.M., 2012, The Geologic Time Scale 2012: Oxford, UK, Elsevier, 1144 p.

Liu, J., Shi, X., Liu, Q., et al., 2014, Magnetostratigraphy of a greigite-bearing core from the South Yellow Sea: Implications for remagnetization and sedimentation: Journal of Geophysical Research, v. 119, p. 7425–7441, https://doi.org/10.1002/2014JB011206.

McFadden, P.L., and McElhinny, M.W., 1990, Classification of the reversal test in palaeomagnetism: Geophysical Journal International, v. 103, p. 725–729, https://doi.org/10.1111/j.1365-246X.1990.tb05683.x.

Minyuk, P.S., Tyukova, E.E., Subbotnikova, T.V., Kazansky, A.Y., and Fedotov, A.P., 2013, Thermal magnetic susceptibility data on natural iron sulfides of northeastern Russia: Russian Geology and Geophysics, v. 54, p. 464–474, https://doi.org/10.1016/j.rgg.2013.03.008.

Passier, H.F., de Lange, G.J., and Dekkers, M.J., 2001, Magnetic properties and geochemistry of the active oxidation front and the youngest sapropel in the eastern Mediterranean Sea: Geophysical Journal International, v. 145, p. 604–614, https://doi.org/10.1046/j.0956-540x.2001.01394.x.

Qiang, X., Xu, X., Zhao, H., and Fu, C., 2018, Greigite formed in Early Pleistocene lacustrine sediments from the Heqing Basin, southwest China, and its paleoenvironmental implications: Journal of Asian Earth Sciences, v. 156, p. 256–264, https://doi.org/10.1016/j.jseaes.2018.01.033.

Roberts, A.P., Chang, L., Rowan, C.J., Horng, C.S., and Florindo, F., 2011, Magnetic properties of sedimentary greigite (Fe_3S_4): an update: Reviews of Geophysics, v. 49, p. RG1002, doi:, https://doi.org/10.1029/2010RG000336.

Roberts, A.P., Cui, Y., and Verosub, K.L., 1995, Wasp-waisted hysteresis loops: mineral magnetic characteristics and discrimination of components in mixed magnetic systems: Journal of Geophysical Research, v. 100, p. 17909–17924, https://doi.org/10.1029/95JB00672.

Stephenson, A., 1980, Gyromagnetism and the remanence acquired by a rotating rock in an alternating-field: Nature, v. 284, p. 48–49, https://doi.org/10.1038/284048a0.

Su, Y.L., Gao, X., Liu, Q.S., Wang, J.B., Haberzettl, T., Zhu, L.P., Li, J.H., Duan, Z.Q., and Tian, L.D., 2013, Mineral magnetic study of lacustrine sediments from Lake Pumoyum Co, southern Tibet, over the last 19 ka and paleoenvironmental significance: Tectonophysics, v. 588, p. 209–221, https://doi.org/10.1016/j.tecto.2012.12.017.

Thibal, J., Etchecopar, A., Pozzi, J.P., Barthès, V., and Pocachard, J., 1999, Comparison of magnetic and gamma ray logging for correlations in chronology and lithology: example from the Aquitanian Basin (France): Geophysical Journal International, v. 137, p. 839–846, https://doi.org/10.1046/j.1365-246x.1999.00828.x.

Tauxe, L., 1998, Paleomagnetic Principles and Practice, Kluwer Acad., Dordrecht, Netherlands.

TABLE DR1. DESCRIPTION OF THE MH CORE

Depth (m)	Lithology
0–2.94	Khaki, grayish yellow silt (0–1.2m contain plant roots) interbedded with grayish green/gray/grayish yellow silty clay; a 2–5 cm salt crust at the surface.
2.94–7.66	Grayish yellow, gray and blackish gray very fine-fine sand with a few plant residues.
7.66–24.6	Blackish gray, grayish yellow medium sand intercalated with thin layers of gray, grayish yellow very fine-fine sand.
24.6–30.8	Blackish gray, grayish yellow fine sand intercalated with thin layers of medium-coarse sand, with horizontal bedding.
30.8–35.2	Grayish yellow, gray-brown pebbly sand interbedded with sandy gravel, with scour surface under the base of the gravel layer. Gravel are poorly sorted, clast-supported, subrounded to rounded with maximum particle diameter of 2–3 cm.
35.2–40.6	Brownish-red, gray, gray-brown and gray-white silty clay, clay intercalated with thin layers of clayey silt; contain horizontal micro-beddings and plant residues.
40.6–45.0	Gray gravel intercalated with thin layers of silty clay, with scour surface under the base of the gravel layer. Gravel are poorly sorted, clast-supported, subrounded to rounded with maximum particle diameter of 5cm.
45.0–48.9	Grayish yellow pebbly sand intercalated with thin layers of silt. Gravel are subrounded to rounded with maximum particle diameter of 5cm.
48.9–50.0	Brownish yellow fine sand.
50.0–53.8	Grayish yellow, gray-white and light red silty clay intercalated with thin layers of sand.
53.8–57.5	Blackish gray medium-coarse sand; contain few granule with particle diameter of 0.2–0.4 cm.
57.5–60.2	Blackish gray, grayish yellow fine sand; with scour surface under the base of the sand layer.
60.2–63.5	Brownish-red, blackish gray and grayish yellow silty clay intercalated with thin layers of sand.
63.5–79.2	Blackish gray, grayish yellow fine sand intercalated with silt and very fine sand, containing parallel and cross beddings.
79.2–80.3	Brownish-red, brownish-yellow and gray-white silt, containing horizontal beddings.
80.3–109.1	Brownish-yellow, grayish-yellow fine sand intercalated with several layers of silt and medium-coarse sand, containing cross beddings.
109.1–111.5	Gray, grayish-yellow sandy gravel. Gravel are clast-supported, subrounded to rounded with maximum particle diameter of 1.5 cm.
111.5–113.1	Grayish-yellow fine sand.
113.1–119.8	Brownish-red, gray, gray-brown and gray-white silt intercalated with thin layers of sand, containing carbonate concretions.
119.8–135.2	Brownish-yellow, grayish-yellow fine sand intercalated with thin layers of silt and medium sand, with internal scour surface under the base of medium sand layer, containing parallel and cross beddings.
135.2–137.5	Grayish-yellow sandy gravel. Gravel are clast-supported, subrounded to rounded with maximum particle diameter of 1.5 cm.
137.5–148.5	Thin- to medium- bedded brownish-yellow, grayish-yellow fine sand interbedded with thin- to medium- bedded medium sand, containing parallel, cross beddings and intraclast.
148.5–175.2	Interbedded layers of medium- to thick- bedded brownish-yellow, grayish-yellow fine sand and medium sand, containing cross beddings and carbonate concretions.
175.2–180.2	Brownish-red, gray, grayish green, grayish brown and gray-white silty clay intercalated with thin layers of sand, containing wavy micro-beddings.
180.2–190.2	Yellowish-red, gray and grayish yellow silt (contain black humus and horizontal beddings) interbedded with grayish-yellow, brownish-yellow fine sand (contain cross beddings and scour surface).
190.2–217.0	Brownish-yellow, grayish-yellow fine sand intercalated with thin- to medium- bedded clay, silt, very fine- and medium- sand, with internal scour surface under the base of sand layer, containing parallel, cross beddings and carbonate concretions.
217.0–218.0	Gray and grayish yellow silt.
218.0–260.0	Brownish-yellow, grayish-yellow fine sand intercalated with thin layers of medium sand, with internal scour surface under the base of some sand layers, containing cross beddings and carbonate concretions.
260.0–270.1	Grayish-yellow gravel intercalated with thin layers of silt and sandy silt, poorly sorted, clast-supported. Gravel are subrounded to rounded with maximum particle diameter of 4.0 cm.
270.1–292.5	Brownish-yellow, grayish-yellow fine sand intercalated with thin layers of silt and medium sand, with internal scour surface under the base of some sand layers, containing intraclast and carbonate concretions.
292.5–299.7	Yellowish-red, light red, gray and grayish yellow silt intercalated with thin layers of grayish-yellow very fine- to fine- sand, containing black humus and horizontal beddings.
299.7–305.1	Brownish-yellow fine sand intercalated with thin layers of medium sand, with scour surface under the base of sand layer, containing cross beddings.
305.1–307.3	Yellowish-red, light red and grayish yellow silt, containing black humus, bioturbation features of burrows, horizontal beddings, and carbonate concretions.
307.3–313.5	Brownish-yellow, grayish yellow fine sand, with scour surface under the base of sand layer.
313.5–318.3	Yellowish-red, light red and grayish yellow silt intercalated with thin layers of grayish-yellow very fine sand, containing black humus and bioturbation features of burrows.
318.3–324.1	Brownish-yellow fine sand intercalated with layers of medium sand, with scour surface under the base of sand layer, containing cross beddings and intraclast.
324.1–327.1	Yellowish-red, light red and grayish yellow silt, containing black humus and horizontal beddings.
327.1–330.1	Brownish-yellow very fine- to fine- sand, containing cross beddings.
330.1–331.8	Brownish-yellow, grayish-yellow and gray pebbly sand, containing cross beddings.
331.8–333.7	Brownish-yellow, grayish-yellow sandy gravel, with scour surface under the base of gravel layer; Gravel are clast-supported, subrounded to rounded with maximum particle diameter of 1.5 cm.
333.7–342.7	Brownish-yellow, grayish-yellow fine sand, containing cross beddings.
342.7–347.6	Yellowish-red, light red and grayish yellow silt intercalated with thin layers of grayish-yellow very fine sand, containing black humus, bioturbation features of burrows and horizontal beddings.
347.6–352.5	Brownish-yellow, grayish-yellow fine sand, containing cross beddings.
352.5–355.0	Light red and grayish yellow silt, containing bioturbation features of burrows and wavy beddings.
355.0–363.0	Brownish-yellow, grayish-yellow fine sand intercalated with layers of very fine and medium sand, with scour surface under the base of sand layer, containing cross beddings.
363.0–365.9	Yellowish-red, light red and grayish yellow silt intercalated with thin layers of grayish-yellow fine sand, containing bioturbation features of burrows and horizontal beddings.
365.9–369.8	Yellowish-red, brownish-yellow and grayish-yellow fine sand, containing cross beddings.
365.9–372.5	Grayish-yellow and gray coarse sand, with scour surface and intraclast under the base of sand layer.
372.5–376.0	Light red and grayish yellow sandy silt and clayey silt intercalated with thin layers of grayish-yellow very fine sand, containing bioturbation features of burrows and horizontal beddings.
376.0–381.2	Brownish-red, brownish-yellow medium- to fine- sand, containing cross beddings.
381.2–383.9	Light red and grayish yellow sandy silt and silt intercalated with thin layers of very fine sand, containing horizontal beddings.
383.9–387.0	Brownish-red fine sand, with scour surface under the base of sand layer.
387.0–390.3	Light red and grayish yellow silt and clayey silt intercalated with thin layers of very fine sand, containing bioturbation features of burrows and horizontal beddings.
390.3–396.2	Brownish-yellow, light yellow fine sand intercalated with thin layers of medium sand, containing parallel and cross beddings.
396.2–417.4	Light red, brownish-red and brownish-yellow silt and clayey silt (containing bioturbation features of burrows and horizontal, wavy, rhythmic, lenticular beddings) intercalated with thin layers of brownish-yellow, light yellow very fine- to fine- sand (containing parallel and flaser beddings, with scour surface and intraclast under the base of some sand layers).
417.4–441.2	Thin- to medium- bedded grayish black, grayish yellow and brownish-yellow fine- to coarse- sand, pebbly sand (containing parallel and flaser

	beddings, with scour surface and intraclast under the base of some sand layers; gravel are subangular to subrounded with maximum particle diameter of 4.0 cm.) interbedded with thin- to medium- bedded light red, brownish-red and brownish-yellow silt and clayey silt (containing bioturbation features of burrows and horizontal, lenticular beddings).
441.2–446.8	Light red, brownish-red and brownish-yellow silt and clayey silt, containing bioturbation features of burrows and horizontal, wavy beddings.
446.8–465.3	Thin- to medium- bedded grayish black, grayish yellow and brownish-yellow very fine- to medium- sand (containing parallel and cross beddings, with scour surface and intraclast under the base of some sand layers) interbedded with thin- to medium- bedded light red, brownish-red and brownish-yellow silt and clayey silt (containing bioturbation features of burrows and horizontal beddings)
465.3–509.4	Light red, brownish-red and brownish-yellow silt and clayey silt (containing bioturbation features of burrows and horizontal, wavy, rhythmic, lenticular beddings) intercalated with thin layers of brownish-yellow, light yellow very fine- to fine- sand (containing parallel and flaser beddings).
509.4–514.5	Grayish yellow, gray coarse- to very coarse- sand and pebbly sand, containing parallel beddings, with scour surface and intraclast under the base of sand layer; gravel are subrounded to rounded with maximum particle diameter of 1.0 cm.
514.5–554.2	Light red, brownish-red and brownish-yellow silt and clayey silt (containing bioturbation features of burrows and horizontal, wavy, rhythmic, lenticular beddings) intercalated with thin layers of brownish-yellow, light yellow very fine- to fine- sand (containing parallel beddings).